Compilation of a glacier inventory for the western Himalayas from satellite data: methods, challenges, and results

Frey, Holger ; Paul, Frank ; Strozzi, Tazio

Abstract: Due to their sensitive reaction to changes in climatic conditions, glaciers have been selected as an essential climate variable (ECV). Although a large amount of ice is located in the Himalayas, this region is yet only sparsely represented in global glacier databases. Accordingly, a sound and comprehensive change assessment or determination of water resources was not yet possible. In this study, we present a new glacier inventory for the western Himalayas, compiled from Landsat ETM+ scenes acquired between 2000 and 2002, coherence images from ALOS PALSAR image pairs, the SRTM digital elevation model (DEM) and the ASTER Global DEM (GDEM). Several specific challenges for glacier mapping were found in this region and addressed. They are related to debris cover, orographic clouds, locally variable snow conditions, and creeping permafrost features in cold-dry regions. Additional to seven topographic parameters that are obtained from the ASTER GDEM for each glacier, we also determined the relative amount of debris cover on the glacier surface. The inventory contains 11,400 glaciers larger than 0.02 km2, which cover a total area of 9,310 km2. Analysis of the inventory data revealed characteristic patterns of mean glacier elevation and relative debris cover amounts that might be related to the governing climatic conditions. The full dataset will be freely available in the GLIMS glacier database to foster further analyses and modeling of the glaciers in this region.

DOI: https://doi.org/10.1016/j.rse.2012.06.020

Remote Sensing of Environment 124, 832–843. 2012.

Compilation of a glacier inventory for the western Himalayas from satellite data: methods, challenges and results

Holger Frey[1] +, Frank Paul[1], Tazio Strozzi[2]

[1]Department of Geography, University of Zurich, Switzerland
[2]Gamma Remote Sensing, Gümligen, Switzerland

[+]Corresponding author (holger.frey@geo.uzh.ch)

Abstract

Due to their sensitive reaction to changes in climatic conditions, glaciers have been selected as an essential climate variable (ECV). Although a large amount of ice is located in the Himalayas, this region is yet only sparsely represented in global glacier databases. Accordingly, a sound and comprehensive change assessment or determination of water resources was not yet possible. In this study, we present a new glacier inventory for the western Himalayas, compiled from Landsat ETM+ scenes acquired between 2000 and 2002, coherence images from ALOS PALSAR image pairs, the SRTM digital elevation model (DEM) and the ASTER Global DEM (GDEM). Several specific challenges for glacier mapping were found in this region and addressed. They are related to debris cover, orographic clouds, locally variable snow conditions, and creeping permafrost features in cold-dry regions. Additional to seven topographic parameters that are obtained from the ASTER GDEM for each glacier, we also determined the relative amount of debris cover on the glacier surface. The inventory contains 11,400 glaciers larger than 0.02 km^2, which cover a total area of 9,310 km^2. Analysis of the inventory data revealed characteristic patterns of mean glacier elevation and relative debris cover amounts that might be related to the governing climatic conditions. The full dataset will be freely available in the GLIMS glacier database to foster further analyses and modeling of the glaciers in this region.

Keywords: Himalaya, glacier inventory, glacier mapping, debris-covered glaciers, coherence images, SRTM, ASTER GDEM, glacier characteristics

1. Introduction

The compilation of glacier inventories from automated multi-spectral classification of optical satellite data in combination with a digital elevation model (DEM) is meanwhile a well-established procedure (e.g. Paul & Kääb, 2005; Andreassen et al., 2008; Racoviteanu et al., 2008; Bhambri & Bolch, 2009; Paul et al., 2009; Racoviteanu et al., 2009; Bolch et al., 2010). There is also no question that a globally complete and detailed glacier inventory is urgently required (e.g. GCOS, 2006; Cogley, 2009; Ohmura, 2009) for a wide range of purposes, among others the modeling of the past and future contribution of glaciers to global sea-level rise (Kaser et al., 2006; Raper & Braithwaite, 2006; Hock et al., 2009), estimation of water resources and hydrological modeling on a regional scale (Koboltsching et al., 2008, Kaser et al. 2010; Huss, 2011), as well as for accurate assessment of glacier changes (e.g. Paul et al., 2004). In particular the latter requires the availability of digital vector lines to refer glacier-specific changes to exactly the same entities.

For the heavily glacierized region of the Himalaya all of the above purposes apply, but little information is available in digital form for a sound change assessment of these glaciers over a large region (Bolch et al., 2012). This results in high uncertainties when local observations need to be generalized (Raina, 2009). Though strong efforts have been made recently to make glacier extents for the Himalaya region available, large parts are still missing in the glacier database of the Global Land Ice Measurements from Space (GLIMS) initiative (cf. Raup et al., 2007). The uncertainties and limited knowledge about the glacier in the Himalayas are obvious from recent debates in the media about the state and future developments of glaciers in this region (Cogley et al., 2010; Schiermeier, 2010). One of the regions with missing glacier outlines is the western Himalayan part of India, which is hence selected as a key region for this study. Glaciers were selected as Essential Climate Variables (ECVs) as they provide some of the clearest evidence of climate change and constitute key variables for early-detection strategies in global climate-related observations (GCOS, 2004). Investigations of glaciers are therefore especially important in regions with sparse climatic records or those where is still under debate whether climate change is occurring or not, such as the western Himalaya (Roy & Balling, 2005; Yadav et al., 2004).

A number of glaciological studies in this region are focusing on individual glaciers or on glacier inventories of smaller sub-basins (e.g., Kulkarni et al., 2007; Bhambri et al., 2011). Mass balance series exist for about a dozen of glaciers in the Indian Himalaya, many of them measured during the 70s to 90s (Raina, 2009). Extensive research has been performed in recent years on Chhota Shigri glacier (e.g. Kumar & Dobhal, 1997; Wagnon et al., 2007; Hasnain et al., 2010), which is part of the mass balance network of the World Glacier Monitoring Service (WGMS) since 2003 (WGMS, 2007). Due to the remoteness and difficult access to many of these glaciers, field observations are very laborious and time consuming. However, satellite data provide an ideal tool to investigate glaciers in this part of the world (Racoviteanu et al., 2008; Bhambri & Bolch, 2009). Besides mapping of glacier outlines, remote sensing techniques were also used for assessing mass balance, volumetric changes and mass loss of Himalayan glaciers (e.g. Kulkarni et al., 2004; Berthier et al., 2007; Matsuo & Heki, 2010). Both Racoviteanu et al. (2008) and Bhambri & Bolch (2009) identified the main challenges of glacier mapping in this region in the lack of a method to accurately delineate glaciers under debris cover, the lack of accurate digital elevation models (DEMs), and restrictions related to the use and export of topographic maps and scientific reports.

There are efforts made by Indian governmental institutions to complete a national glacier inventory (Raina & Shrivastava, 2008; Sangewar & Shukla, 2009), which partly includes inventory work already compiled for several basins (e.g. Kaul, 1999, Vohra, 2010). These inventories are in tabular form, including topographic information such as minimum and maximum elevation, mean elevation of accumulation and ablation region, maximum glacier length, mean width, area, accumulation area ratio (AAR), and an estimation of mean depth and resulting glacier volume. Glacier outlines were obtained from topographic maps with additional information from aerial photography and satellite imagery if available. But as these outlines are not available in a digital form (Braithwaite, 2009), it is difficult to assess the quality and accuracy of these datasets. In many cases, reports and research as well as the source maps based on which these inventories were compiled are not published or even

classified (Bhambri & Bolch, 2009). For the Himachal Pradesh and Uttaranchal states, digital glacier outlines were compiled by the International Center for Integrated Mountain Development (ICIMOD) using data from the Indian Remote Sensing Satellite series 1D (IRS1D) and topographic maps (ICIMOD, 2007). A new glacier inventory covering almost the entire Hindu-Kush, Karakoram, and Himalayas, has recently been compiled by ICIMOD (Bajracharya & Shresta, 2011), but the respective digital outlines are not yet available. Hence, an assessment of glacier changes based on the existing dataset is hardly possible as they differ regarding format, source data, acquisition method, analysts, and mapping purpose (cf. Racoviteanu et al., 2009). For the reasons above, any derived changes in glacier area might be more artificial rather than real (Racoviteanu et al., 2009; Paul & Hendriks, 2010; Bolch et al., 2012).

To overcome the major shortcomings of this situation, we here present a new digital glacier inventory that is derived from satellite data using semi-automated mapping techniques and now publically available. For the special challenges in this region such as heavily debris-covered glacier tongues combined with high solar elevation (reducing image contrast), frequent orographic clouds, seasonal snow, and glaciers ending in regions with permafrost, best effort approaches are presented to solve them. In particular, we apply a recently introduced new technique for improved delineation of debris-covered glaciers with coherence images from the ALOS PALSAR sensor (Atwood et al. 2010, Strozzi et al. 2010). The data analysis demonstrates the potential of the datasets and includes glacier parameters per river basin. By making the vector data sets of the resulting glacier outlines freely available through the GLIMS glacier database, more specific analyses or individual research questions can be performed and addressed. The focus of this study is thus on the methodological aspects of generating a state-of-the-art inventory for more than 10,000 glaciers in a region with challenging mapping conditions.

2. Study region and data

2.1. Extent of the glacier inventory

The study region is located in the western Himalayas and covers an area of more than 100,000 km^2. It reaches from the town of Kargil near Srinagar to the Tehri dam and the Alaknanda basin (Fig. 1). The northern limit is defined by the Indus, the southeastern limit by the Dhauli Ganga River. Several sub-basins of both the Indus (Jhelum, Chenab, Shyok, Ravi, Sutlej, and Gar Zangbo) and Ganges (Yamuna, Bhagirati, and Alaknanda) are included. The study region contains the parts of the Ladakh Range south of Indus, the Zanskar Range and parts of the Garhwal Himalaya.

Fig. 1

Mid-latitude westerlies bring the main precipitation to the study region and can produce heavy snowfalls in winter (Böhner, 2006; Hatwar et al., 2005). This results in decreasing precipitation from the Indus-Ganges lowlands towards the Tibetan Plateau (Bookhagen & Burbank, 2006). The study region is located at the end of monsoonal conveyor belt, and is thus sensitive to the strength of the Indian summer monsoon (Bookhagen et al., 2005). In normal years, the influence of the monsoon is comparably low (Bolch et al., 2012), but in abnormal monsoon years such as 2002 and 2010 it can cause exceptionally strong rainfall events in the normally arid northern parts of the study region (Bookhagen et al., 2005; Juyal, 2010).

2.2. Satellite scenes

The USGS archive (http://glovis.usgs.org) was inspected to find Landsat scenes of the study region with as low snow and cloud cover as possible to be suitable for glacier mapping. We selected eight appropriate scenes from the Landsat ETM+ sensor acquired in 2000 (three scenes), 2001 (three) and 2002 (two) in good temporal agreement with the acquisition of the SRTM DEM. Due to complementary cloud cover, two scenes were chosen for path 147 / row 37. Table 1 gives an overview on the satellite data used in this study. To facilitate the mapping of debris-covered glaciers parts, coherence images were created from four ALOS PALSAR image pairs (cf. Section 3.2.). The sequential ALOS PALSAR scenes have been

acquired from the ascending orbit in Fine-Beam Dual mode (FBD - HH/HV) with a 275 m baseline and a 46 day time interval during the snow-free period in 2007 (cf. 3.2. and Table 1).

Table 1

On the pre-processing stage, we downloaded the selected Landsat ETM+ scenes and generated different color composites (RGB 321 for near true-color images and RGB 543 for discriminating clouds, ice, snow and debris). In the USGS archive, all scenes are in Universal Transverse Mercator (UTM) projection, with the scene center coordinates defining the zone. The scenes in our study region belong to UTM zones 43N and 44N and for practical purposes we decided to have the mosaiced inventory in a single UTM zone (43N).

2.3. Digital Elevation Models

A DEM of appropriate quality and resolution is required to separate individual glaciers along their drainage divides, and to derive specific topographic inventory parameters such as minimum, maximum, mean, and median elevation, mean slope, and mean aspect (Paul et al., 2009). For the study region, no local or national DEM with sufficient quality is publicly available. However, with the DEM from the Shuttle Radar Topography Mission (SRTM) and the ASTER GDEM, there are two elevation datasets available that cover almost the entire world, at least outside the polar regions, and that are accurate enough for compiling topographic glacier inventory data (Frey & Paul, 2012). The SRTM DEM was acquired using radar interferometry (InSAR) (Farr et al., 2007), which is subject to data voids in rugged high-mountain terrain due to radar shadow and layover effects. The Consultative Group for International Agriculture Research (CGIAR) compiled a void-free version (SRTM3v4) by interpolating the terrain in data voids based on information from other elevation datasets (Reuter et al., 2007). This void-free SRTM version has been used in numerous glaciological studies, mainly related to the assessment of ice volume variations with time (e.g. Surazakov and Aizen, 2006; Berthier et al., 2007; Schiefer et al., 2007; Paul & Haeberli, 2008). The dataset is available in 5 by 5 degree tiles; tile 'srtm_52_06' covers the entire study region and was used here. The ASTER GDEM was compiled by applying automated photogrammetric techniques to all suitable scenes available from the ASTER data archive (Hayakawa et al., 2008) and has a spatial resolution of 30 m. To cover the entire study region, 16 ASTER GDEM tiles with 1 by 1 degree coverage were downloaded and mosaiced.

In a study for the Swiss Alps Frey & Paul (2012) found, that over glaciers, the SRTM DEM acquired with InSAR is slightly superior to the photogrammetric ASTER GDEM, but both datasets can be used for the compilation of glacier inventories. However, a subtraction of the ASTER GDEM from the SRTM DEM revealed in many regions differences of several hundred meters up to 1.5 km (Fig. 2a). As the large differences are congruent with the data void mask of the SRTM DEM that is provided by CGIAR along with SRTM3v4 data, these differences are likely caused by erroneous interpolations in the SRTM data voids. In the hillshade views of the DEMs (Figs. 2b and 2c), this becomes clearly visible: the interpolated terrain in the SRTM DEM is continuous and looks realistic, but all the interpolated regions are systematically too low, resulting in distinct shadows in the hillshade view at the margins of these crater-like depressions. The mean difference of the two elevation models outside the SRTM data voids is -0.4 ± 26.8 m, but -234.1 ± 284.6 m in regions with interpolated SRTM data. We thus used the ASTER GDEM instead of the SRTM DEM for this study, as the gross errors would degrade the quality of the topographic parameters and result in a wrong location of the drainage divides. However, for the processing of the ALOS PALSAR coherence images (cf. 3.2.), the SRTM DEM was applied to remove the topography-related phase shifts and for geocoding. This is because the artificial bumps and holes of the ASTER GDEM are introducing artifacts that are nearly impossible to be detected and removed. Furthermore, the SRTM DEM has a validity mask that was applied to the coherence images before analyzing them for terrain properties.

Fig. 2

3. Methods

3.1. Mapping of clean ice

On the main processing stage, we computed band ratios of band 3 (green, TM3) and band 5 (short wave infrared (SWIR), TM5), with a specific threshold applied to each scene to map clean ice and snow (Paul et al., 2002; Paul et al., 2009; Bolch et al., 2010). Due to the rather strong contrast between ice/snow and rock/debris, the mapping result was not very sensitive to changes of the thresholds and values between 1.9 and 2.1 were chosen for the different scenes. This small range is also related to the relatively high sun elevation at these low latitudes (in all scenes the sun elevation at acquisition was between 55° and 63°), which results in only small regions in cast shadow. As a last step of the main processing, a median filter with 3 x 3 kernel-size was applied to reduce noise, i.e. to eliminate isolated pixels and fill small gaps in glacier-covered regions (Paul et al., 2002).

The more time-consuming part of the glacier mapping was required in the post-processing stage, where all misclassifications were manually corrected within a Geographic Information System (GIS). This includes elimination of erroneously classified features like turbid water surfaces (lakes and wide rivers), clouds and remaining snow avalanche deposits, as well as delineating of debris-covered glacier parts (cf. Section 3.2.). Paul et al. (2009) report that under good conditions glaciers of 0.01 km^2 can be identified in imagery with 15 – 30 m resolution. Considering the large amount of snow patches outside of glaciers in the scenes processed here, the minimum size to be registered for the inventory was set to 0.02 km^2, which equals about 22 Landsat ETM+ pixels. The same size threshold was also chosen for the new glacier inventory of ICIMOD (Bajracharya & Shresta, 2011).

In particular on the southern margin of the Himalayan range, orographic clouds are prevalent due to uplift of moisture transported by winds from the southwest. These clouds cover glaciers partly or entirely and make their complete mapping often impossible. In some cases we used overlapping neighboring scenes or a scene from another date to map the hidden glaciers or missing parts. To keep track of the source scene for each glacier, the image ID of the source satellite image has been included in the database. A few glaciers have been affected by clouds in all scenes, and therefore have been excluded from further analyses.

3.2. Mapping of debris-covered glacier parts

Editing of debris-covered glacier parts is one of the most time-consuming tasks in the compilation of a glacier inventory and highly error prone (e.g. Bolch et al., 2008; Racoviteanu et al., 2008; Bhambri et al., 2011). In higher latitudes, illumination differences caused by the convex shape of the tongues or the break in slope at the contact to lateral moraines can be used to track glacier boundaries (cf. Paul et al., 2004). However, the high sun elevation in the relatively low latitudes of the study region leads to low contrasts in the satellite images and makes the identification of the glacier margins and terminuses more difficult.

The coherence of interferograms from radar images can be used to accurately map glacier margins under debris cover (Atwood et al., 2010; Strozzi et al., 2010). The degree of coherence is a measure of the phase noise of the interferogram. It depends on sensor parameters (wavelength, polarization, system noise, slant range resolution), parameters related to the imaging geometry (interferometric baseline, local incidence angle), and target parameters. Volume scattering and temporal change (i.e. random motion of the scatterers, change of the scatterers) decrease the degree of coherence. The system- and geometry-dependent effects can be taken into account by appropriate interferometric processing. The decorrelation caused by volume scattering and temporal change, on the other hand, is important to characterize the target properties. During summer time, most of the seasonal snow has disappeared and ice flow and melting are the main factors of surface-geometry changes, which lead to a decrease of the coherence.

The SAR processing of the ALOS PALSAR data included radiometric calibration for the antenna gain and slant range distance, radio frequency interference filtering, and common band filtering of the azimuth and range spectra. The resulting single look complex (SLC) images were well focused and allowed to produce interferograms of high quality after accurate co-registration of master and slave images (e.g. Ulaby et al., 1982). The

interferometric processing combined pairs of SLC images at HH-polarization into an interferogram using a GAMMA Remote Sensing in-house software. Because of rugged areas, a simulated phase image, which corresponds to the topographic phase, was first computed from the void-filled SRTM DEM and then subtracted from the interferometric phase. For coherence estimation an adaptive window size was used. In the first step, the coherence was estimated with a fixed, relatively small window size. In the second step, the window size was determined based on the first estimate, applying larger windows in order to estimate lower coherence. The estimator window size was varied between 3 x 3 and 9 x 9 pixels for a 4 azimuth-looks interferogram. In addition, a weighting function, decreasing linearly with increasing distance, was applied (Wegmüller & Werner, 1996). With this procedure reliable values at the pixel level were found without compromising the spatial resolution. The resulting terrain-corrected and geocoded coherence images were combined with a mask considering regions with layover and radar shadow as well as the SRTM voids.

As shown in Fig. 3, glaciers (clean and debris-covered parts) and water bodies show very low coherence values (dark) due to the change in the geometrical configuration of the scatterers. Since the identification and exclusion of water bodies is straightforward with the optical satellite scenes, the identification of the moving glaciers is strongly facilitated by these coherence images. However, due to data gaps and disturbances like water bodies and mass movements in non-glaciated terrain, an automated mapping from the coherence images alone is not possible. We thus used them as a background to guide the manual editing.

Fig. 3

Due to the cold-arid climate in the northeastern part of the study region, glacier tongues end in permafrost and rock glaciers are abundant at elevations above ~4000 m a.s.l. with annual precipitation less than 1000 mm (Owen & England, 1998). It is often hard to discriminate between forms of creeping scree and debris-covered glacier tongues as they exhibit a similar surface structure and identical spectral properties. In addition, these features are a mix of glacial and periglacial forms and simple differentiations between debris-covered glaciers and rock glaciers are even on-site not possible (e.g. Whalley et al., 1986; Haeberli et al., 2006). Some hints in interpreting these features are provided by the InSAR coherence images; however, not only glacier flow but also the movement of rockglaciers and other creeping features causes a loss of coherence (Fig. 4b).

As a consequence, the following criteria were applied for the glacier mapping north of the main range: rockglaciers were not considered for this inventory, although they can contain a considerable amount of ice and are therefore interesting freshwater resources (e.g. Azócar & Brenning, 2009). This is justified as the aim of the study is to map the Essential Climate Variable (ECV) 'glaciers and ice caps' as defined by the Global Climate Observing System (GCOS). In this regard, rockglaciers are part of 'permafrost and seasonally-frozen ground' (GCOS, 2006). In some cases typical structures of the surface like elongated features of debris-covered glacier tongues or lobes on rockglaciers, respectively, were used to guide the delineation, in other cases the extent of the glacier tongue was directly extracted from the coherence image (Fig. 4).

Fig. 4

The separate mapping of clean ice areas (automated) and debris-covered glacier parts (manual delineation) allows a later straightforward distinction of debris-covered and debris-free regions. To keep record of this information, the amount of debris-covered glacier area on the total glacier area is stored for each glacier in the attribute table.

3.3. Delineation of ice divides

To get the extent of individual glaciers, the manually edited glacier map has to be separated along the hydrologic divides. This delineation of the ice divides has a major impact on the areas of the individual glaciers and therefore on many subsequent analyses (Beedle et al., 2008). For compiling the drainage divides, we first followed the automated approach described by Bolch et al. (2010) and derived the hydrological basins by watershed analysis with the DEM that had been clipped to a buffer of 700 m around the glacier outlines. A

comparison of this drainage divides with the satellite imagery revealed larger discrepancies in the accumulation region, e.g. many sliver polygons along the glacier margins (Fig. 5). Furthermore, many glaciers are already separated by steep, snow and ice-free rock ridges and, thus, do not need to have a further divide. We hence decided to digitize the drainage divides manually using the automatically derived hydrological basins only as a guide. Additionally, we used a hillshade view, a flowdirection raster of the DEM and the satellite scenes for interpretation. In situations where ridges were recognizable in the satellite image due to illumination differences, the divides were drawn surrounding them as the information from the satellite image was considered to be superior to the DEM.

Fig. 5

After intersecting the glacier outlines with the drainage divides, individual glacier entities are obtained and glacier-specific parameters could be calculated for all polygons larger than 0.02 km^2. Besides an internal ID and the aforementioned percentage of debris-cover, the ID of the source scene, the area, and topographic parameters (minimum-, maximum-, mean- and median elevation, mean slope, and mean aspect in degree and mean aspect sector, (Paul et al., 2009)) were assigned to each glacier

4. Results

In total, 11,436 mapped glaciers larger than 0.02 km^2, covering a total area of 9,313 km^2 were included in the inventory. The distribution of glaciers per basin is shown in Fig. 6 and Table 2 gives a basin-wise summary of selected glacier parameters.

Fig. 6
Table 2

The distribution of glaciers by number and by area per size class (Fig. 7a) and per mean aspect sector (Fig. 7b) shows the typical patterns of mountain glaciers in mid-latitudes (e.g. Paul et al., 2011; Andreassen et al., 2008; Bhambri et al., 2011): In this region, 86% of all analyzed glaciers are smaller than 1 km^2, but they share only 20.2% of the total area. On the other hand, the 13 largest glaciers cover more than 11% of the glacierized area (1012 km^2). Analyzing mean elevation versus aspect sector (small circles in Fig. 7b) reveals 100 m higher values in eastern sectors (NE, E, SE) than in western sectors (SW, W, NW) (5361 and 5268 m a.s.l., respectively).

Fig. 7

We found that nearly 15% (1,326 km^2) of the glacier area is debris-covered. Debris-free (debris-covered) areas have an overall mean elevation of 5323 m a.s.l. (4755 m a.s.l.) with a and their mean slope value is 22.5° (15.4°). All glaciers larger than 3.8 km^2 are partly debris-covered (with only one exception). This confirms the previously made observation that debris cover occurs mainly on the low-lying and less inclined tongues of large valley glaciers (Paul et al., 2004; Shukla et al., 2010).

The distribution of glacier area by elevation (i.e. the hypsometry) of all analyzed glaciers is depicted in Fig. 8. Besides the total glacier surface, individual graphs for clean and debris-covered ice are shown as well. Although more than 85% of the total glacier area is debris free, the amount of debris-covered glacier parts is dominant below 4400 m a.s.l.

Fig. 8

Mean elevation is a very good approximation for the balance-budget ELA and thus a suitable parameter to analyze the governing climatic conditions (e.g. Le Bris et al., 2011; Bolch et al., 2012). This climate dependence becomes obvious when looking at the spatial distribution of the glacier-specific mean values (Fig. 9): at the southwestern margin of the Himalayan main range, the relatively maritime climate results in mean elevations below 4300 m a.s.l., whereas

in the Tibetan Plateau northeast of the main range mean elevations are mostly above 5700 m a.s.l., reflecting the cold-dry climatic conditions.

Fig. 9

By cutting glaciers at their median elevation, a separate analysis of the upper and the lower half is possible. As expected, debris cover predominantly occurs in the lower glacier parts (23.1% of the lower glacier parts are covered with debris), only 3.1% of the debris cover occurs above median elevation. Furthermore, considerably lower mean slope values were found for the lower glacier halves (16.8°) than for the upper glacier halves (25.9°).

5. Discussion

5.1. Glacier inventory data

The total number of mapped glaciers (11,436) depends on the minimum size threshold (here 0.02 km^2). If this value is set to 0.05 km^2, the number of glaciers is only 8,676. Sangewar & Shukla (2009) report the total number of Indian glaciers with a size larger than 0.05 km^2 (including further parts of the Uttarakhand and the entire Sikkim and Arunachal Himalaya) to be 9,575. This difference indicates that probably several small glaciers were not included in the Indian inventory and/or that some glaciers have been disintegrating into smaller glaciers during retreat. Of course, there is also some variability in the number due to the differences in interpretation of such small features as (perennial) ice or (seasonal) snow.

Kääb (2005) observed in a study about the Bhutan Himalaya that glaciers south of the main range exhibit a considerably higher amount of debris-covered area than northbound glaciers. To investigate whether this gradient in debris cover exists also in our study region, we averaged the individual relative amounts of debris cover for the mean elevation classes as shown in Fig. 9 (the amount of average relative debris cover per elevation class is given in the legend). The amount of debris cover also shows this gradient, from 20% in the southwest (mean elevation < 4500 m a.s.l.) to only 6% in the northeast (mean elevation > 5550 m a.s.l.). The suggested explanation of more intensive debris supply from the steep rock faces surrounding the glaciers in the south might apply here too, and differences in geology as well influence the amount of debris-cover. However, the high amount of debris cover on low-elevation glacier parts can also be caused by the insulating effect of the debris itself, i.e. an auto-correlation effect.

According to the generalized flow law for ice (assumption of perfect plasticity), the ice thickness at flat glacier parts is higher than at steep parts (Patterson, 1994). From this point of view the ice in the comparably flat lower parts of the larger valley glaciers is much thicker than the ice in the steep higher glacier reaches. In other words, a large amount of the glacier volume is stored in the low-lying ablation regions, as median elevation separates glaciers in two halfs of equal size. This implies that large amounts of ice can become subject to melt in the near future. And although melting is expected to be reduced under the debris cover on these lower glacier parts (e.g. Benn & Lehmkuhl, 2000), the surface properties possibly have only limited influence on the melting: In their study in the Himachal Pradesh, Berthier et al. (2007) observed the strongest lowering of glacier surfaces at low elevations, independent of the amount of debris cover; Gardelle et al. (2012) made similar findings in the Karakoram, Bolch et al. (2008) in the Mt. Everest region, and Paul & Haeberli (2008) in the European Alps.

Avalanche-fed glaciers are a special glacier type of this region (Benn & Lehmkuhl, 2000; Bolch et al., 2012). The tongues of such glaciers are located under steep slopes and are mainly fed by ice and snow avalanches, but otherwise they might be completely separated from their accumulation region, resulting in two (or more) disconnected polygons in the inventory. An automatic assignment of such separated glacier tongues to their respective higher reaches is not possible. Such glaciers tend to be less sensitive to climatic changes (e.g. Iturrizaga, 2011), and most topographic parameters lose their validity. As it is difficult to identify them, an exact number cannot be given, we assume that there are probably more than hundred of them spread over the study region.

5.2. Debris cover mapping with coherence images

The use of ALOS PALSAR coherence images acquired during summer proved to be very helpful as they strongly facilitated the identification of the (moving) debris-covered tongues. Especially the large valley glaciers in the main range and on the western part of the study region with extensive debris cover could be mapped much more efficiently and precisely by using this information. However, generating coherence images requires specific software and skills, and possible data procurement costs of the raw scenes need to be considered. As the coherence images always contain data voids in steep and mountainous topography, automated glacier mapping based solely on such data is difficult for this region. This finding is in contrast to the study of Atwood et al. (2010), who have been successful in mapping all glaciers in sub-regions of the Wrangell Mountains and the Juneau Ice Field in Alaska from coherence imagery alone. Nevertheless, this combination of optical and microwave remote sensing data is very promising as the precision of the digitized outlines is higher and more consistent. It might be expanded in the future to other regions and other purposes, such as the identification of glaciers under persistent orographic cloud cover. Summer coherence images computed from SAR images of other sensors characterized by shorter wavelengths and acquisition time intervals like TerraSAR-X or Cosmo-SkyMed are an alternative to ALOS PALSAR. The relatively long acquisition time interval of ERS and ENVISAT data, on the other hand, results in a strongly reduced distinction between debris-covered glaciers and the surrounding non-moving areas. The approach of first mapping clean ice and then adding debris-covered glacier parts allows separating these two surface types. This provides valuable information for various modeling applications concerning for example the modeling of future glacier development (Quincey et al., 2007) and melt water production (e.g., Huss et al., 2008; Kaser et al., 2010). Coherence images have the potential to be also used for the mapping of rock glaciers, but this must be verified first. The related tests should consider images with different time lags, spatial resolution, and possibilities to discriminate rock glaciers from other creeping features based on field evidence.

5.3. Accuracy

For clean glaciers without debris cover, an uncertainty of ±1 pixel (30 m) is assumed for the outline position, since comparisons of the applied automated mapping method to reference data sets have proven that the approach yields to accurate results (cf. Paul & Kääb, 2005; Andreassen et al., 2008). Larger uncertainties can occur in shadowed regions and for glacier divides (ice – ice margins) in accumulation regions, but the latter have no influence on the total area of multi-part glacier ensembles. A quantitative assessment of the accuracy of the glacier outlines of debris-covered glacier parts is hardly possible as no ground truth is available. The precision of the outlines has been estimated in a multi-digitizing experiment with three analysts, by comparing the outlines from different digitizations relative to each other, revealing a standard deviation of the relative area differences below 3%. The position of the outlines shows partly large variations, in particular between the different analysts. For glaciers that are partly debris-covered we therefore assigned a local uncertainty of ±2 pixels (60 m). In most cases, the differences at the margins along the glacier tongue were smaller than this value, but larger for the glacier terminus. These results are confirmed by a large multi-digitizing experiment in the European Alps, Alaska and the Himalayas (Paul et al., subm.). For debris-covered glaciers in the north, which are often merged with periglacial forms (see 3.2. and Fig. 4), a local uncertainty value of ±5 pixels (150 m) was assigned.

The ASTER GDEM used here is affected by small-scale artifacts like pits and bumps that are characteristic for this dataset (METI/NASA/USGS, 2009). Such errors can have a strong influence on the topographic parameters minimum and maximum elevation, as these values are obtained from individual DEM cells; for the other parameters the DEM values are averaged over the entire glacier area, and artifact-related deviations average out (Frey & Paul, 2012). A quantitative assessment of these errors was not possible as no other independent DEM of sufficient quality is available for this purpose and the SRTM DEM could not be used for such an analysis due to the gross artifacts in the interpolated data voids. However, in the applied workflow the mapping process is separated from the processing steps that require a DEM. Hence, a fast reprocessing of drainage divides or topographic parameters or both would be possible, if a suitable DEM of higher quality becomes available.

Although SRTM was not used for the compilation of the glacier inventory, the errors of the void-filled SRTM version (see Section 2.3.) nevertheless affected the results in two ways: first, our coherence images have large data voids (Fig. 3), as the topographic phase of the SAR scenes could not be removed in the error-affected regions. The second influence is related to the geolocation accuracy of the satellite scenes and therefore the absolute positional uncertainty of the glacier outlines. As described in the metadata files of the Landsat scenes, the orthorectification of these satellite images was performed with the Global Land Survey (GLS) DEM, which consists of void-filled SRTM data from CGIAR in our study region (USGS, 2008). Locally, we found pixels that were more than 5 pixels (150 m) shifted away from their location indicated by the drainage divides derived from the ASTER GDEM. It is difficult to evaluate this effect more quantitatively as the shift depends on elevation, the elevation error, and, due to the cross track scanning of Landsat, on the distance of the pixel from the center (nadir) line of the scene (e.g. Schowengerdt, 2007).

5.4. Outlook

Due to its high degree of detail and completeness as well as the large area covered, the datasets generated in this study can provide a baseline for future change assessment and more detailed investigations of climate change impacts on glaciers in the Himalayas. Considering the availability of earlier Landsat data including Multi-Spectral Scanner (MSS) scenes from the 1970s, a remote sensing-based assessment of glacier changes over a time span of almost 40 years would be possible. Vohra (2010) mentioned that several MSS scenes with suitable conditions for glacier terminus mapping are available. As the presented dataset is a snapshot of the situation between 2000 and 2002, glacier changes of the last decade can be determined as well, once more recent satellite scenes become available. For the mapping of debris-covered glacier tongues the spatial resolution of MSS (68 x 83 m) might be too coarse, but use of images with lower solar elevation might partly compensate for this. Declassified imagery of spy sensors from the 60s like Corona or Hexagon provide a valuable alternative for such change assessment and were already successfully applied in the study region by Bhambri et al. (2011).

For the related change assessments, several challenges have to be considered (see also Paul & Hendriks, 2010; Racoviteanu et al., 2009): the two datasets that are compared must have the same level of detail, i.e. they should be compiled using the same methodology and source information of identical quality. A repeat inventory should thus also be compiled from satellite data with comparable spatial resolution and spectral properties. Furthermore, a comparison of total glacier areas is hampered by changing conditions in steep headwalls covered by snow, ice and avalanche deposits (cf. Fig. 3) that are prevalent in the Himalayas. Bhambri & Bolch (2009) also expect that an area comparison without consideration of the changing conditions in the accumulation area would lead to larger area variations than ‘real’ changes of glacier extent.

Additional data compilation as well as modeling and field studies are required in the future to get a better understanding of the interactions of Himalayan glaciers with climate and also to model the potential future behavior of these glaciers. In this regard, it also needs to be assessed to which degree models that were developed and calibrated for other glacier regions can be transferred to and applied in this region, as the topographic and glacier characteristics are partly very different from other mid-latitude mountain ranges.

6. Conclusions

Several conclusions can be drawn from this study. They are related to the application of well-established and recently developed glacier mapping techniques to a large region with challenging conditions as well as the large extent and high degree of completeness of this new inventory, that allowed, in combination with the analysis of topographic parameters, new findings about the characteristics of the glaciers in this region. They can be summarized as:

- In a high-mountain region in the western Himalayas with a total area of about 100,000 km^2, more than 10,000 glaciers larger than 0.02 km^2 and covering an area of almost

10,000 km^2 were mapped by a semi-automated mapping technique based on eight Landsat ETM+ scenes acquired between 2000 and 2002.

- About 15% of the total glacier area is debris-covered. In average, debris cover is restricted to less inclined glacier parts and found at lower elevations. In the elevation band between 3200 and 4400 m a.s.l. the amount of debris-covered glacier parts exceeds the clean ice areas.
- Across the Himalayan range, from the southwest to the northeast, an increase of mean glacier elevation by about 1500 m and a decrease in the amount of relative debris cover from 22% to 6% were observed, reflecting the different governing climatic and topographic conditions.
- Ablation regions have much gentler slopes than accumulation regions, indication that most of the ice volume in the region is located at low elevations.
- The most laborious task for glacier mapping was the manual delineation of debris-covered glacier parts, which was strongly facilitated by the coherence images from microwave sensors. Differentiation between debris-covered glacier parts and creeping features in permafrost was particularly challenging for the northbound glaciers under cold-arid climate conditions.
- The void-filled SRTM DEM revealed gross artifacts in interpolated data voids and was thus considered to be unsuitable for this region. Therefore, the ASTER GDEM was used to compile drainage divides along which individual glaciers were separated. The latter was also used to calculate glacier-specific topographic parameters.

This inventory is a baseline dataset for various future studies, including change assessment, modeling of future glacier development and related changes in river-runoff of the Ganges and Indus as well as estimates of the potential sea-level rise contribution. The entire dataset is freely available from GLIMS glacier database for these and other purposes.

Acknowledgements

The ASTER GDEM is a product of METI and NASA; SRTM is a product of NASA, the void-filled version used in this study is produced by CGIAR-CSI. Landsat scenes were provided by the USGS; ALOS PALSAR data courtesy AOPOL.4086, © JAXA. This study has been funded by the ESA project GlobGlacier (21088/07/I-EC) and the EU FP7 project HighNoon (grant no. 227087).

References

Andreassen, L., Paul, F., Kääb, A., & Hausberg, J. (2008). Landsat-derived glacier inventory for Jotunheimen, Norway, and deduced glacier changes since the 1930s. *The Cryosphere, 2*(2), 131-145.

Atwood, D. K., Meyer, F., & Arendt, A. (2010). Using L-band SAR coherence to delineate glacier extent. *Canadian Journal of Remote Sensing, 36*(1), 186-195.

Azócar, G. F., & Brenning, A. (2009). Hydrological and geomorphological significance of rock glaciers in the dry Andes, Chile (27°-33°S). *Permafrost and Periglacial Processes*, *21*, 42–53. doi:10.1002/ppp.669

Bajracharya, S. R., & Shresta, B. (Eds.). (2011). The Status of Glaciers in the Hindu Kush-Himalayan Region. Kathmandu: ICIMOD.

Beedle, M. J., Dyurgerov, M., Tangborn, W., Khalsa, S. J. S., Helm, C., Raup, B., Armstrong, R., et al. (2008). Improving estimation of glacier volume change: a GLIMS case study of Bering Glacier System, Alaska. *The Cryosphere*, *2*, 33-51.

Benn, D. I. & Lehmkuhl, F. (2000). Mass balance and equilibrium-line altitudes of glaciers in high-mountain environments. *Quaternary International, 65/66,* 15-26.

Berthier, E., Arnaud, Y., Kumar, R., & Ahmad, S. (2007). Remote sensing estimates of glacier mass balances in the Himachal Pradesh (Western Himalaya, India). *Remote Sensing of Environment, 108*, 327-338.

Bhambri, R., & Bolch, T. (2009). Glacier mapping: a review with special reference to the Indian Himalayas. *Progress in Physical Geography, 33*(5), 672-704. doi: 10.1177/0309133309348112

Bhambri, R., Bolch, T., Chaujar, R. K., & Kulshreshtha, S. C. (2011). Glacier changes in the Garhwal Himalaya, India, from 1968 to 2006 based on remote sensing. *Journal of Glaciology, 57*(203), 543-556.

Böhner, J. (2006). General climatic controls and topoclimatic variations in Central and High Asia. *Boreas, 35*, 279-295.

Bolch, T., Buchroithner, M., Pieczonka, T., & Kunert, A. (2008). Planimetric and volumetric glacier changes in the Khumbu Himal, Nepal, since 1962 using Corona, Landsat TM and ASTER data. *Journal of Glaciology, 54*(187), 592-600.

Bolch, T., Menounos, B., & Wheate, R. (2010). Landsat-based inventory of glaciers in western Canada, 1985–2005. *Remote Sensing of Environment, 114*, 127-137.

Bolch, T., Kulkarni, A., Kääb, A., Huggel, C., Paul, F., Cogley, J. G., Frey, H., Kargel, J. S., Fujita, K., Scheel, M., Bajracharya, S., & Stoffel, M. (2012). The State and Fate of Himalayan Glaciers. *Science, 336*(6079), 310-314. doi:10.1126/science.1215828

Bookhagen, B., & Burbank, D. W. (2006): Topography, relief, and TRMM-derived rainfall variations along the Himalaya. *Geophysical Research Letters, 33*, L08405.

Bookhagen, B., Thiede, R. C., & Strecker, M. R. (2005). Abnormal monsoon years and their control on erosion and sediment flux in the high, arid northwest Himalaya. *Earth and Planetary Science Letters, 231*, 131-146. doi:10.1016/j.epsl.2004.11.014

Braithwaite, R.J. (2009). Review. Raina, V.K. and D. Srivastava, Glacier atlas of India. *Journal of Glaciology, 55*(193), 938.

Cogley, J. G. (2009). A more complete version of the World Glacier Inventory. *Annals of Glaciology, 50*(53), 32–38.

Cogley, J. G., Kargel, J. S., Kaser, G., & van der Ween, C. J. (2010). Tracking the source of glacier misinformation. *Science, 327*(5965), 522-522.

Farr, T. G., Rosen, P. A., Caro, E., Crippen, R., Duren, R., Hensley, S., Kobrick, M., Paller, M., Rodriguez, E., Roth, L., Seal, D., Shaffer, S., Shimada, J., Umland, J., Werner, M., Oskin, M., Burbank, D., & Alsdorf, D. (2007). The shuttle radar topography mission. *Reviews in Geophysics, 45*(2), 1-33.

Frey, H., & Paul, F. (2012). On the suitability of the SRTM DEM and ASTER GDEM for the compilation of topographic parameters in glacier inventories. *International Journal of Applied Earth Observations and Geoinformation*, *18*, 480–490. doi:10.1016/j.jag.2011.09.020

Gardelle, J., Berthier, E., & Arnaud, Y. (2012). Slight mass gain of Karakoram glaciers in the early twenty-first century. *Nature Geoscience, 5*, 322-325. doi:10.1038/ngeo1450

GCOS (2004). *Implementation plan for the global observing system for climate in support of the UNFCCC*. GCOS Reports - 92 (WMO/TD No. 1219), 136 pp.

GCOS (2006). *Systematic observation requirements for satellite-based products for climate - Supplemental Details to the GCOS Implementation Plan*. GCOS Reports - 107 (WMO/TD No. 1338), 91 pp.

Haeberli, W., Hallet, B., Arenson, L., Elconin, R., Humlum, O., Kääb, A., Kaufmann, V., Ladanyi, B., Matsuoka, N., Springman, S., & Vonder Mühll, D. (2006). Permafrost creep and rock glacier dynamics. Permafrost and Periglacial Processes, 17(3), 189–214. doi:10.1002/ppp.561

Hasnain, S.I., Kumar, R., Ahmad, S, & Tayal, S. (2010). A study of selected glaciers under the changing climate regime. In R.S. Williams & J.G. Ferrigno (Eds.), *Satellite image atlas*

of glaciers of the world. Denver, CO, United States Geological Survey, F259-F274. (USGS Professional Paper 1386-F)

Hatwar, H. R., Yadav, B. P., & Rama Rao Y. V. (2005). Prediction of western disturbances and associated weather over western Himalayas. *Current Science, 88*(6), 913-920.

Hayakawa, Y. S., Oguchi, T., & Lin, Z. (2008). Comparison of new and existing global digital elevation models: ASTER G-DEM and SRTM-3. *Geophysical Research Letters, 35*(17), L17404. doi:10.1029/2008GL035036

Hock, R., De Woul, M., Radić, V., & Dyurgerov, M. (2009). Mountain glaciers and ice caps around Antarctica make a large sea-level rise contribution. *Geophysical Research Letters, 36*(7), L07501. doi:10.1029/2008GL037020

Huss, M. (2011). Present and future contribution of glacier storage change to runoff from macroscale drainage basins in Europe. *Water Resources Research, 47*(7), W07511. doi:10.1029/2010WR010299

Huss, M., Farinotti, D., Bauder, A., & Funk, M. (2008). Modelling runoff from highly glacierized alpine drainage basins in a changing climate. *Hydrological Processes, 22*(19), 3888–3902. doi:10.1002/hyp.7055

ICIMOD (2007). Inventory of Glaciers, Glacial Lakes and Identification of Potential Glacial Lake Outburst Floods (GLOFs) Affected by Global Warming in the Mountains of Himalayan Region. *DVD-ROM*.

Iturrizaga, L. (2011). Trends in 20th century and recent glacier fluctuations in the Karakoram Mountains. *Zeitschrift für Geomorphologie, 55*(3), 205-231. doi:10.1127/0372-8854/2011/0055S3-0059

Juyal, N. (2010). Cloud burst-triggered debris flows around Leh. *Current Science, 99*(9), 1166-1167.

Kääb, A. (2005). Combination of SRTM3 and repeat ASTER data for deriving alpine glacier flow velocities in the Bhutan Himalaya. *Remote Sensing of Environment, 94*(4), 463-474.

Kaser, G., Cogley, J., Dyurgerov, M., Meier, M., & Ohmura, A. (2006). Mass balance of glaciers and ice caps: Consensus estimates for 1961–2004. *Geophysical Research Letters, 33*(19), L19501. doi:10.1029/2006GL027511

Kaser, G., Grosshauser, M., & Marzeion, B. (2010). Contribution potential of glaciers to water availability in different climate regimes. *Proceedings of the National Academy of Sciences, 107*, 20223-20227.

Kaul, M.K. (1999). *Inventory of the Himalayan glaciers: a contribution to the International Hydrological Programme*. Kolkata: Geological Survey of India, 165 pp. (Geological Survey of India, Special Publication, No. 34)

Koboltschnig, G. R., Schöner, W., Zappa, M., Kroisleitner, C., & Holzmann, H. (2008). Runoff modelling of the glacierized Alpine Upper Salzach basin (Austria): multi-criteria result validation. *Hydrological Processes, 22*, 3950-3964.

Kulkarni, A. V., Rathore, B. P., & Alex, S. (2004). Monitoring of glacial mass balance in the Baspa basin using accumulation area ratio method. *Current Science, 86*(1), 101-106.

Kulkarni, A. V., Bahuguna, I. M., Rathore, B. P., Singh, S. K., Randhawa, S. S., Sood, R. K., & Dhar, S. (2007). Glacial retreat in Himalaya using Indian Remote Sensing satellite data. *Current Science, 92*(1), 69-74.

Kumar, S., & Dobhal, D. P. (1997). Climatic effects and bed rock control on rapid fluctuations of Chhota Shigri glacier, northwest Himalaya, India. *Journal of Glaciology, 43*(145), 467-472.

Le Bris, R., Paul, F., Frey, H., & Bolch, T. (2011). A new satellite-derived glacier inventory for western Alaska. *Annals of Glaciology, 52*(59), 135-143.

Matsuo, K., & Heki, K. (2010). Time-variable ice loss in Asian high mountains from satellite gravimetry. *Earth and Planetary Science Letters, 290*(1-2), 30-36.

METI, NASA, & USGS. (2009). ASTER GDEM Validation Summary Report, 28 p.

Ohmura, A. (2009). Completing the World Glacier Inventory. *Annals of Glaciology, 50*(53), 144-148.

Owen, L. A., & England, J. (1998). Observations on rock glaciers in the Himalayas and Karakoram Mountains of northern Pakistan and India. Geomorphology, 26, 199–213.

Paterson, W. (1994). The physics of glaciers. New York: Pergamon Press.

Paul, F., & Kääb, A. (2005). Perspectives on the production of a glacier inventory from multispectral satellite data in Arctic Canada: Cumberland Peninsula, Baffin Island. *Annals of Glaciology, 42*, 59-66.

Paul, F., & Haeberli, W. (2008). Spatial variability of glacier elevation changes in the Swiss Alps obtained from two digital elevation models. *Geophysical Research Letters, 35*(21), L21502. doi: 10.1029/2008GL034718

Paul, F., & Hendriks, J. (2010). Area change detection of glaciers. In: P. Pellikka, & W.G. Rees (Eds.), *Remote Sensing of Glaciers - Techniques for Topographic, Spatial and Thematic Mapping of Glaciers*. Leiden: CRC Press, Taylor and Francis Group, 137-152.

Paul, F., Kääb, A., Maisch, M., Kellenberger, T., & Haeberli, W. (2002). The new remote-sensing-derived Swiss glacier inventory: I. Methods. *Annals of Glaciology, 34*, 355-361.

Paul, F., Huggel, C., & Kääb, A. (2004). Combining satellite multispectral image data and a digital elevation model for mapping of debris-covered glaciers. *Remote Sensing of Environment, 89*(4), 510-518.

Paul, F., Barry, R. G., Cogley, J. G., Frey, H., Haeberli, W., Ohmura, A., Ommanney, C. S. L., Raup, B., Rivera, A., & Zemp, M. (2009). Recommendations for the compilation of glacier inventory data from digital sources. *Annals of Glaciology, 50*(53), 119-126.

Paul, F., Frey, H., & Le Bris, R. (2011). A new glacier inventory for the European Alps from Landsat TM scenes of 2003: challenges and results. *Annals of Glaciology*, *52*(59), 144–152.

Paul, F., Barrand, N., Berthier, E., Bolch, T., Casey, K., Frey, H., Joshi, S. P., Konovalov, V., Le Bris, R., Moelg, N., Nosenko, G., Nuth, C., Pope, A., Racoviteanu, A., Rastner, P., Raup, B., Scharrer, K., Steffen, S., Winsvold, S. (subm.). On the accuracy of glacier outlines derived from remote sensing data. *Annals of Glaciology*.

Quincey, D. J., Richardson, S. D., Luckman, A., Lucas, R. M., Reynolds, J. M., Hambrey, M. J., & Glasser, N.F. (2007). Early recognition of glacial lake hazards in the Himalaya using remote sensing datasets. *Global and Planetary Change, 56*(1-2), 137-152.

Racoviteanu, A. E., Williams, M. W., & Barry, R. G. (2008). Optical remote sensing of glacier characteristics: a review with focus on the Himalaya. *Sensors, 8*, 3355-3383. doi: 10.3390/s8053355.

Racoviteanu, A., Frank, P., Bruce, R., Khalsa, S., & Armstrong, R. (2009). Challenges and recommendations in mapping of glacier parameters from space: results of the 2008 Global Land Ice Measurements from Space (GLIMS) workshop, Boulder, Colorado, USA. *Annals of Glaciology, 50*(53), 53–69.

Raina, V. (2009). Himalayan Glaciers - A State-of-Art Review of Glacial Studies, Glacial retreat and Climate Change. *Ministry of Environments and Forests – Discussion Paper*. 60 p.

Raina, V. K., & Srivastava, D. (2008). *Glacier atlas of India*. Bangalore: Geological Society of India, 316 pp.

Raper, S., & Braithwaite, R. (2006). Low sea level rise projections from mountain glaciers and icecaps under global warming. *Nature, 439*, 311–313. doi:10.1038/nature04448

Raup, B., Kääb, A., Kargel, J. S., Bishop, M. P., Hamilton, G., Lee, E., Paul, F., Rau, F., Soltesz, D., Khalsa, S. J. S., Beedle, M., & Helm, C. (2007). Remote sensing and GIS technology in the Global Land Ice Measurements from Space (GLIMS) Project. *Computers & Geosciences, 33*, 104-125.

Reuter, H., Nelson, A., & Jarvis, A. (2007). An evaluation of void filling interpolation methods for SRTM data. *International Journal of Geographic Information Science, 21*(9), 983–1008.

Roy, S. S., & Balling R. C. (2005). Analysis of trends in maximum and minimum temperature, diurnal temperature range, and cloud cover over India. *Geophysical Research Letters, 32*(12), L12702. doi:10.1029/2004GL022201

Sangewar, C. V., & Shukla, S. P. (2009). Inventory of the Himalayan Glaciers: A Contribution to the International Hydrological Programme. *Special Publication, Geological Survey of India, 34*: An Updated Edition, 594 p.

Schiefer, E., Menounos, B., & Wheate, R. (2007). Recent volume loss of British Columbian glaciers, Canada. *Geophysical Research Letters, 34*(16), L16503. doi: 10.1029/2007GL030780.

Schiermeier, Q. (2010). Glacier estimate is on thin ice. *Nature, 463*(7279), 276-277.

Schowengerdt, R. A. (2007). *Remote sensing – Models and methods for image processing* (Third edition). Amsterdam : Academic Press, 515 pp.

Shukla, A., Arora, M. K., & Gupta, R. P. (2010). Synergistic approach for mapping debris-covered glaciers using optical–thermal remote sensing data with inputs from geomorphometric parameters. *Remote Sensing of Environment, 114*(7), 1378–1387. doi:10.1016/j.rse.2010.01.015

Strozzi, T., Paul, F., & Kääb, A. (2010). Glacier mapping with ALOS PALSAR within the GlobGlacier project. *Proceedings of the ESA Living Planet Symposium 2010, 28. June – 02 July 2010, Bergen, Norway*.

Surazakov, A. B., & Aizen, V. B. (2006). Estimating volume change of mountain glaciers using SRTM and map-based topographic data. *IEEE Transactions on Geoscience and Remote Sensing, 44*(10), 2991-2995.

Ulaby, F. T., Moore, R. K., & Fung, A. K. (1982). *Microwave Remote Sensing: Active and Passive*. Vol. II. *Radar Remote Sensing and Surface Scattering and Emission Theory*. Addison-Wesley, Reading, Massachusetts.

USGS (2008). *Global Land Survey Digital Elevation Model (GLSDEM)*. Global Land Cover Facility, University of Maryland, College Park, Maryland. (http://www.glcf.umd.edu/data/glsdem/description.shtml, accessed June 2012)

Vohra, C. P. (2010): Glaciers of India – A brief overview of the state of glaciers in the Indian Himalaya in the 1970s and the end of the 20th century. In R.S. Williams & J.G. Ferrigno (Eds.), *Satellite image atlas of glaciers of the world.* Denver, CO, United States Geological Survey, F259-F274. (USGS Professional Paper 1386-F).

Wagnon, P., Linda, A., Arnaud, Y., Kumar, R., Sharma, P., Vincent, C., Pottakkal, J. G., Berthier, E., Ramanathan, A., Hasnain, S. I., & Chevallier, P. (2007). Four years of mass balance on Chhota Shigri Glacier, Himachal Pradesh, India, a new benchmark glacier in the western Himalaya. *Journal of Glaciology, 53*(183), 603-611.

Wegmüller, U., & . Werner, C. (1996). Land applications using ERS-1/2 tandem data. *Proceedings of the Fringe 96 Workshop: ERS SAR Interferometry, Zurich, 30 September - 2 October 1996, ESA SP-406,* 97-112.

WGMS (2007). *Glacier Mass Balance Bulletin No. 9 (2004-2005)*. W. Haeberli, M. Hoelzle, & M. Zemp (Eds.), ICSU(FAGS)/IUGG(IACS)/UNEP/UNESCO/WMO, World Glacier Monitoring Service, Zurich, 100 pp.

Whalley, W. B., Marin, H. E., & Gellatly, A. F. (1986). The problem of "hidden" ice in glacier mapping. *Annals of Glaciology, 8*, 181-183.

Yadav, R. R., Park, W.-K., Singh, J., & Bhasha, D. (2004). Do the western Himalayas defy global warming? *Geophysical Research Letters, 31*(17). doi:10.1029/2004GL020201

Figure captions

Fig. 1: Overview of the study region, satellite data and location of figures, map in the top right corner shows the surrounding territories. Dashed rectangles indicate the outlines of the coherence images.

Fig. 2: (a) Difference of SRTM – ASTER GDEM for the whole extent of the ASTER GDEM mosaic. Red areas (void-filled SRTM up to 1.5 km lower than ASTER GDEM) are congruent with data voids in the SRTM raw version. The black rectangle indicates the location of the hillshade views shown in (b) and (c) (with illumination coming from northwest). (b) Zoom to the hillshade view of SRTM. (c) Zoom to the hillshade view of ASTER GDEM. Note the artifacts in the SRTM DEM, causing the large differences shown in (a). The dark parts at margins of the interpolated data voids are shadow areas caused by the fall of the terrain of several hundred meters.

Fig. 3: Mapping of debris-covered glacier parts by using coherence images in the region of Chhota Shigri (the north-facing glacier east of the image center). The long debris-covered tongue on the eastern part of the image is Bara Shigri glacier. Red lines show the raw glacier outlines resulting from the ETM3/ETM5 ratio; corrected glacier outlines are shown in yellow. (a) False-color composite of the ETM+ scene (RGB 543). (b) Coherence image from two ALOS PALSAR scenes. Note the low coherence (dark pixels) over glacier areas, independent of the amount of debris cover. Data voids (blue areas) are large, but normally they are restricted to steep terrain and do not affect the glacier tongues. Also the water area in front of the terminus of Bara Shigri results in decorrelation; however, water can easily be discriminated in the optical satellite image (a).

Fig. 4: Challenging mapping situation in the dry-cold north of the study region where glacier tongues lay in the zone of continuous permafrost. White lines represent the raw glacier outlines after thresholding the ETM3/ETM5 ratio image (i.e. the clean ice areas); yellow lines delineate the maximum extent of the features with a glacier-tongue shape, including rock glaciers and potential non-moving dead ice parts. The corrected glacier outlines of the inventory are shown in red. The background is a false-color composite (RGB 543) of the ETM+ scene (a), and the coherence image of an ALOS PALSAR image pair (with no-data areas shown in blue) (b).

Fig. 5: Basins derived from SRTM (blue lines), ASTER GDEM (white lines), and the manually corrected final basins (red lines). Many glaciers are already completely isolated by ridges and do not need to be separated by drainage divides (box A). Besides many sliver polygons along the margins in the upper parts of glaciers at some places large differences occur between basins derived from SRTM and ASTER GDEM (box B).

Fig. 6: Map of hydrological basins and the inventoried glaciers. Asterisks indicate basins that are only partly covered by the inventory.

Fig. 7: Distribution of the number of glaciers (dark grey), glacier area (light grey), and mean glacier elevation (circles). (a) Per size class. (b) Per aspect sector.

Fig. 8: Hypsometry of all glaciers of the study region. Clean ice in blue, debris-covered glacier parts in brown, and total glacier are in black.

Fig. 9: Mean glacier elevation and relative amount of debris cover is spatially correlated: Mean elevation is increasing from southwest to northeast, whereas the debris cover (indicated by the number in brackets in the legend) is decreasing along this gradient.

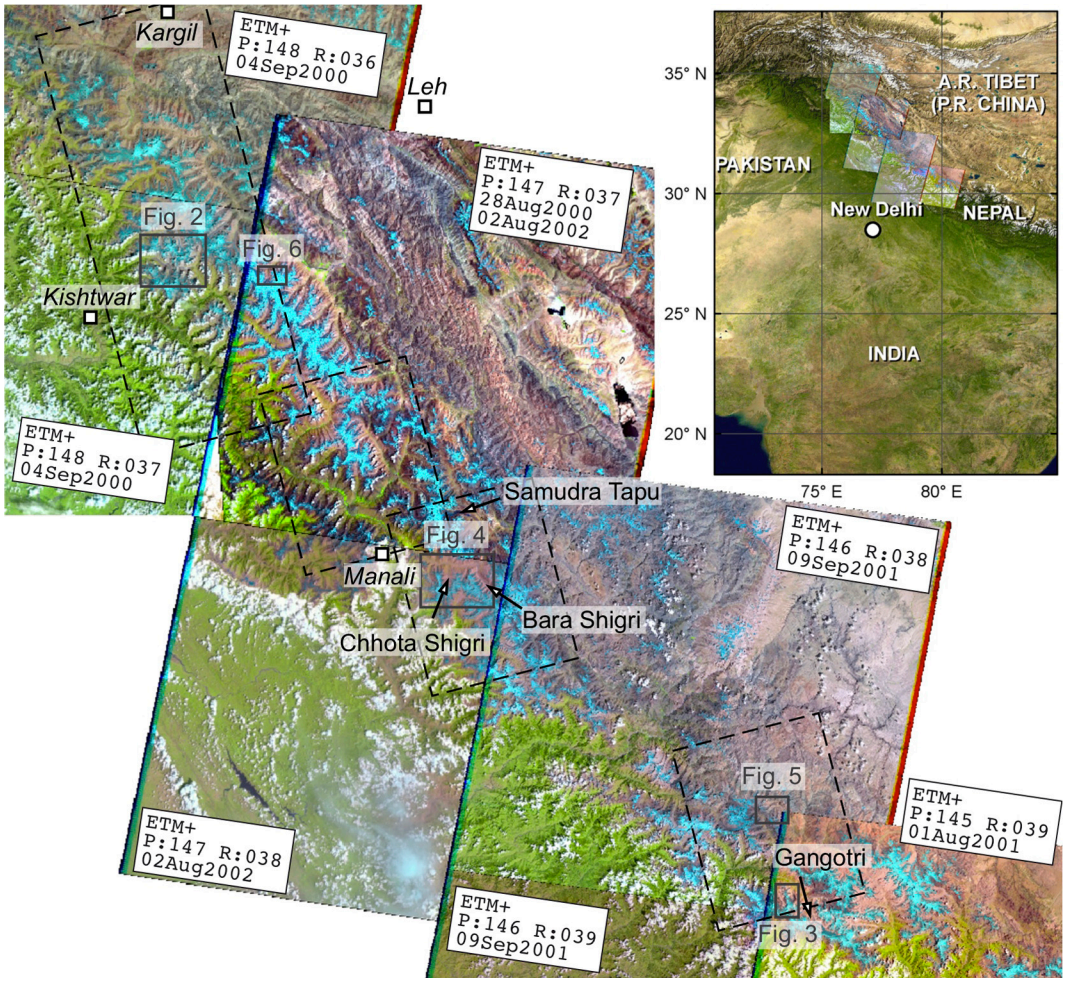
Kargil
ETM+
P:148 R:036
04Sep2000
Leh
ETM+
P:147 R:037
28Aug2000
02Aug2002
Fig. 2
Fig. 6
Kishtwar
ETM+
P:148 R:037
04Sep2000
Samudra Tapu
Fig. 4
Manali
Bara Shigri
Chhota Shigri
ETM+
P:146 R:038
09Sep2001
Fig. 5
ETM+
P:145 R:039
01Aug2001
Gangotri
Fig. 3
ETM+
P:147 R:038
02Aug2002
ETM+
P:146 R:039
09Sep2001
35° N
30° N
25° N
20° N
75° E
80° E
A.R. TIBET
(P.R. CHINA)
PAKISTAN
New Delhi
NEPAL
INDIA

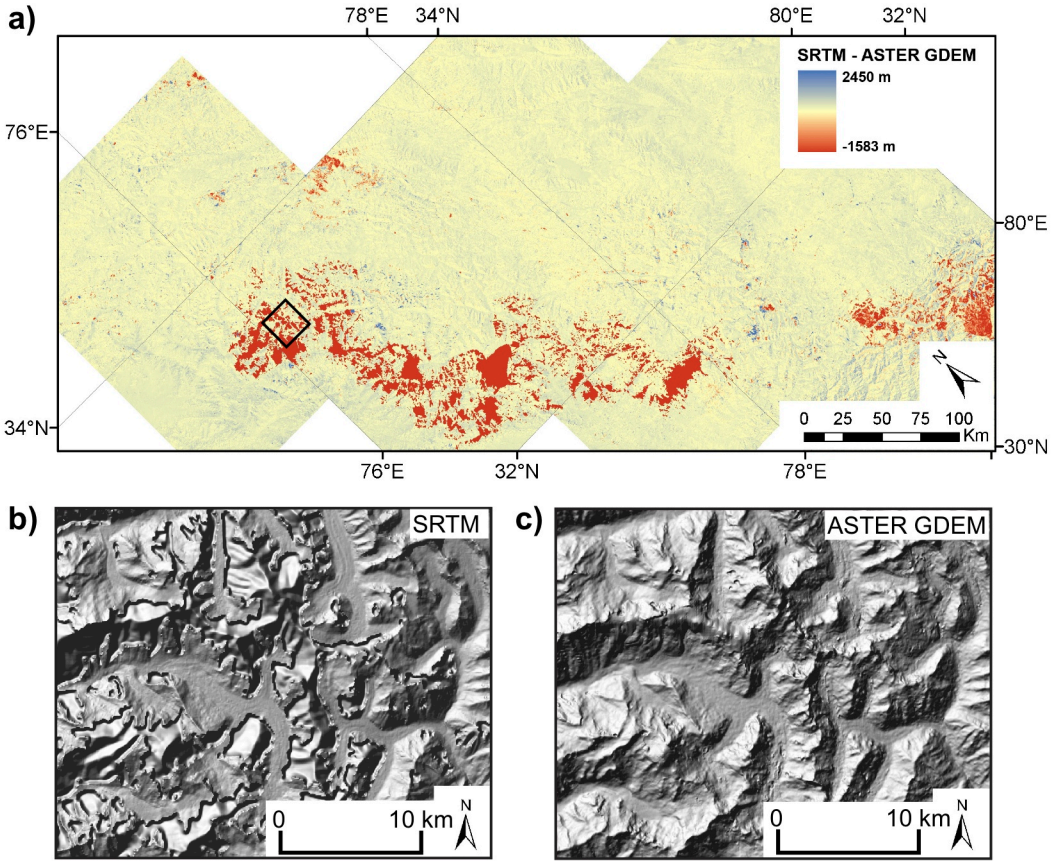
a)
78°E
34°N
80°E
32°N
SRTM - ASTER GDEM
2450 m
-1583 m
76°E
80°E
34°N
30°N
76°E
32°N
78°E
N
0 25 50 75 100
Km
b)
SRTM
0
10 km
N
c)
ASTER GDEM
0
10 km
N

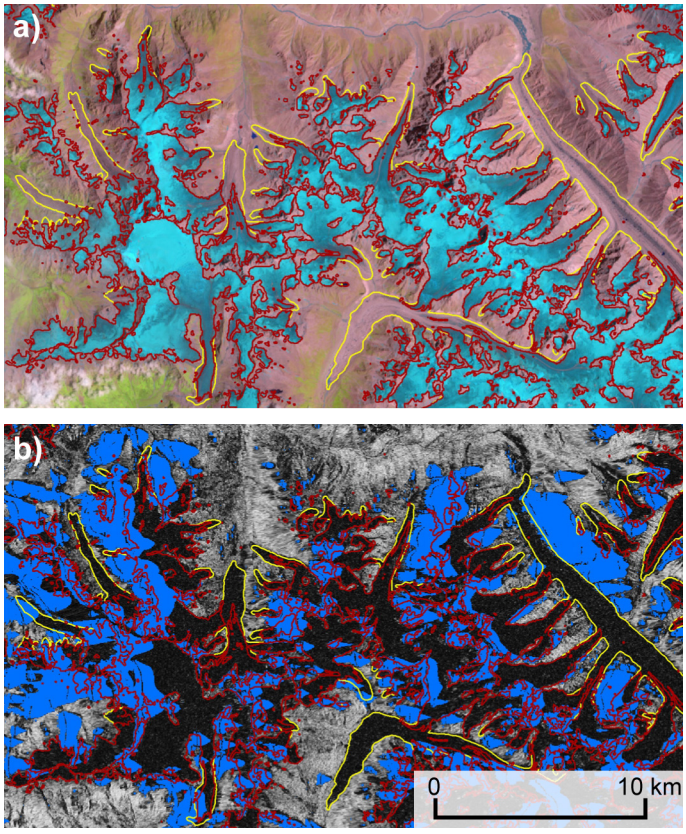
a)
b)
0
10 km

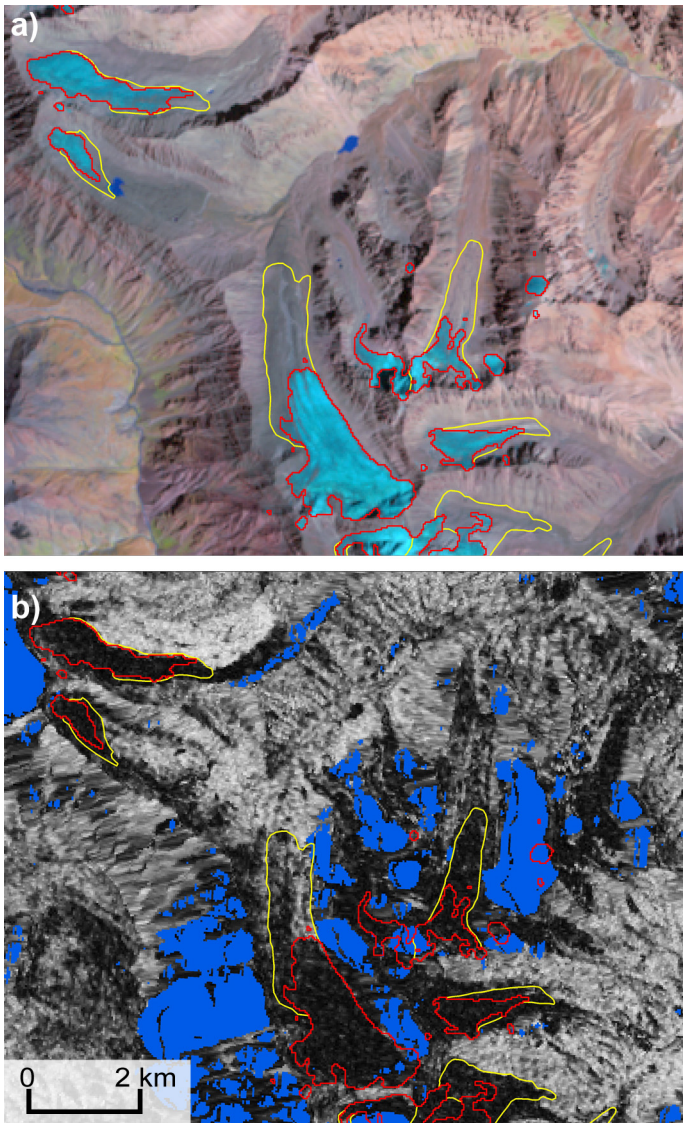
a)
b)
0
2 km

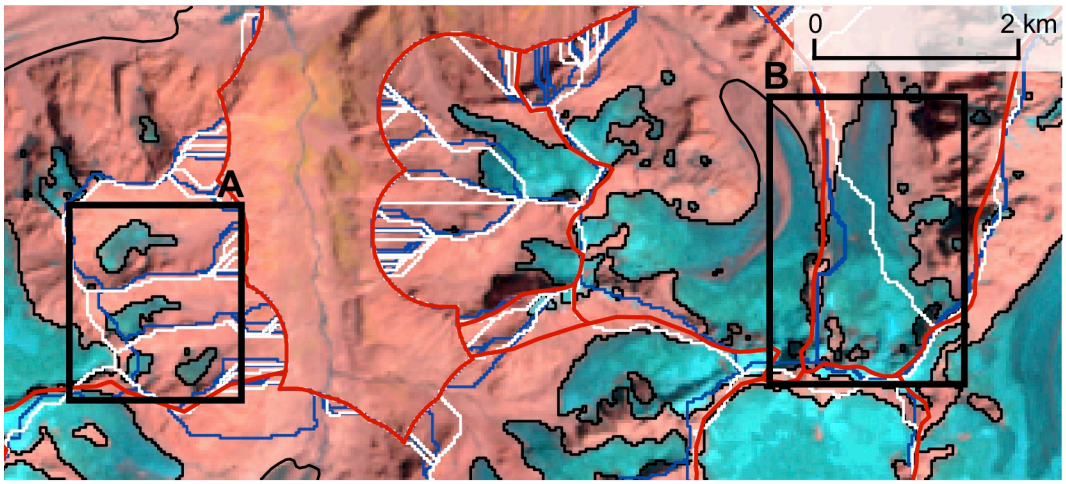
0
2 km
A
B

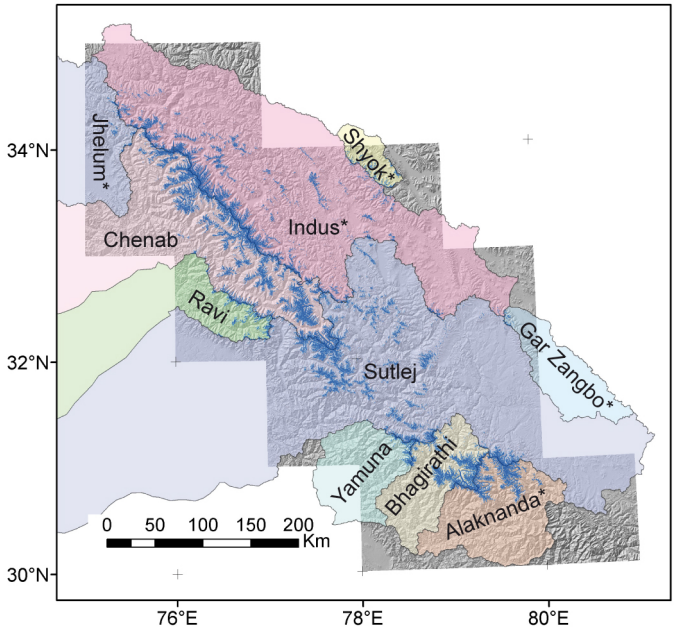
Jhelum*
Shyok*
Chenab
Indus*
Ravi
Gar Zangbo*
Sutlej
Yamuna
Bhagirathi
Alaknanda*
0 50 100 150 200
Km
34°N
32°N
30°N
76°E
78°E
80°E

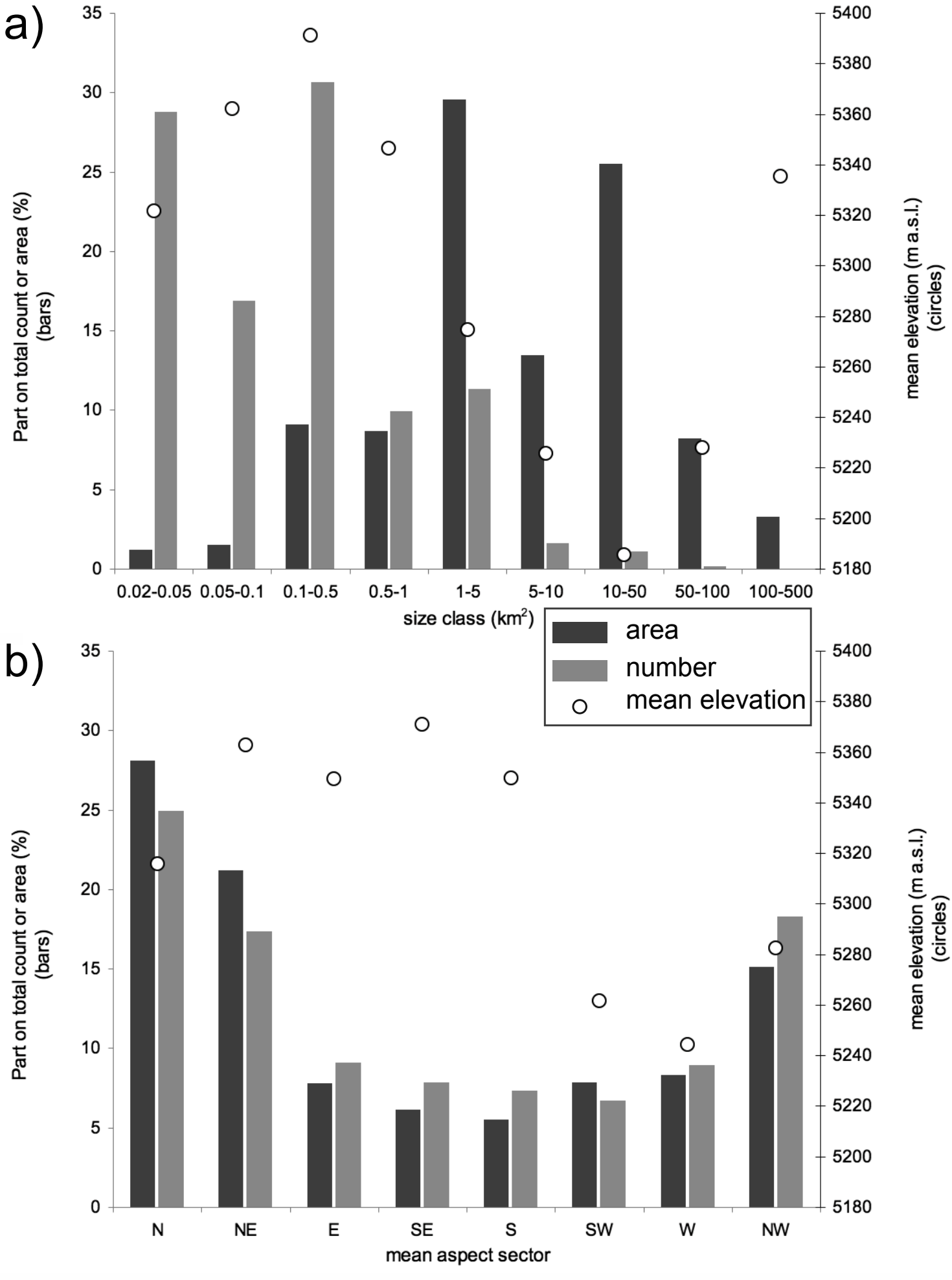
a)
b)
Part on total count or area (%) (bars)
mean elevation (m a.s.l.) (circles)
0
5
10
15
20
25
30
35
5180
5200
5220
5240
5260
5280
5300
5320
5340
5360
5380
5400
0.02-0.05
0.05-0.1
0.1-0.5
0.5-1
1-5
5-10
10-50
50-100
100-500
size class (km²)
area
number
mean elevation
N
NE
E
SE
S
SW
W
NW
mean aspect sector

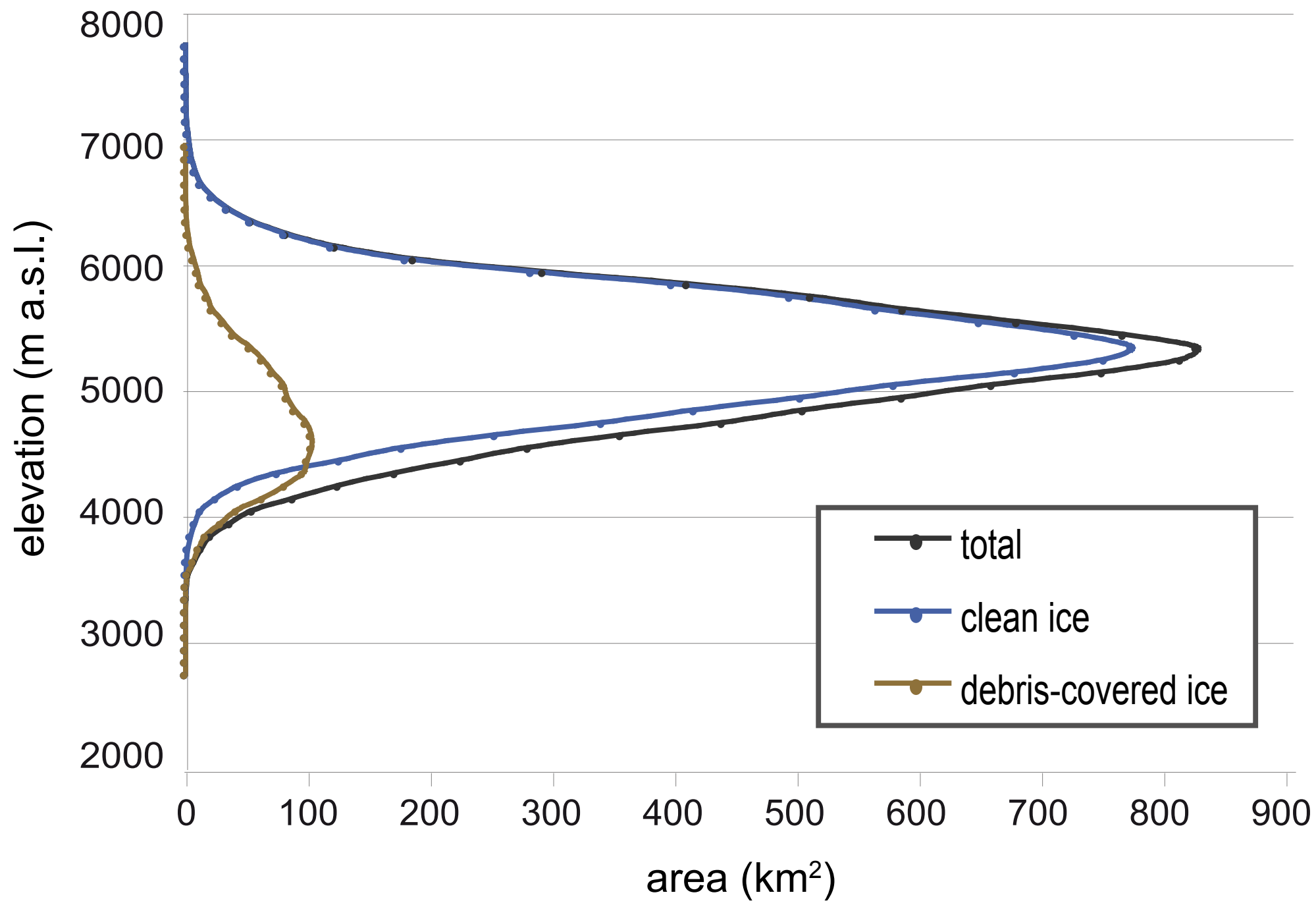
8000
7000
6000
5000
4000
3000
2000
elevation (m a.s.l.)
0
100
200
300
400
500
600
700
800
900
area (km²)
total
clean ice
debris-covered ice

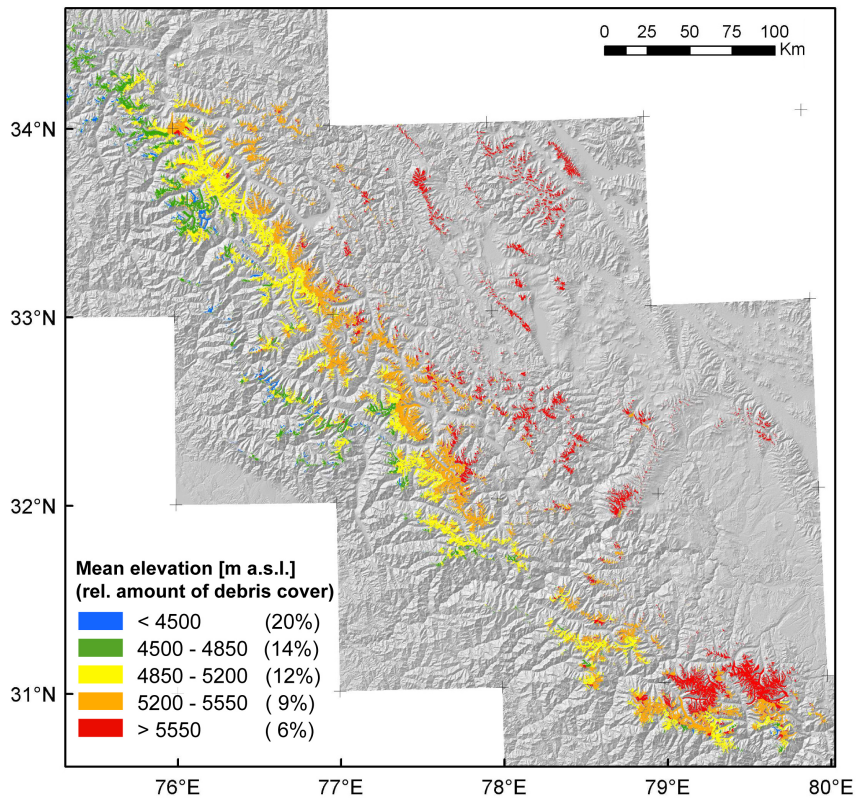
0 25 50 75 100
Km
34°N
33°N
32°N
31°N
76°E
77°E
78°E
79°E
80°E
Mean elevation [m a.s.l.]
(rel. amount of debris cover)
< 4500 (20%)
4500 - 4850 (14%)
4850 - 5200 (12%)
5200 - 5550 (9%)
> 5550 (6%)

Tables

Table 1: List of used satellite data.

Purpose	Platform and sensor	ID (P=path, R=row, T=Track, F=Frame, B=Baseline)		Date (dd/mm/yyyy)
Glacier mapping	Landsat ETM+	P:145 R:039		01/08/2001
	Landsat ETM+	P:146 R:038		09/09/2001
	Landsat ETM+	P:146 R:039		09/09/2001
	Landsat ETM+	P:147 R:037		28/08/2000, 02/08/2002
	Landsat ETM+	P:147 R:038		02/08/2002
	Landsat ETM+	P:148 R:036		04/09/2000
	Landsat ETM+	P:148 R:037		04/09/2000
Coherence images	ALOS PALSAR	T:525 F:650-670	B:275m	12/07/2007, 27/08/2007
	ALOS PALSAR	T:524 F:640	B:46m	10/08/2007, 25/09/2007
	ALOS PALSAR	T:523 F:630	B:270m	27/07/2007, 08/09/2007
	ALOS PALSAR	T:521 F:610	B:-216m	05/08/2007, 20/09/2007

Table 2: Glacier parameters per basin

Basin	No of glaciers	Glacier area (km^2)	Min. elevation (m a.s.l.)	Max. elevation (m a.s.l.)	Mean elevation (m a.s.l.)	Median elevation (m a.s.l.)	Mean slope (°)	Deb. cover (%)**
Jhelum*	170	69	4268	4588	4432	4434	25.5	12
Indus*	3,095	2,191	5234	5578	5404	5402	25.4	9
Chenab	2,774	3007	4842	5299	5064	5064	27.9	16
Shyok*	271	107	5705	6027	5868	5867	26.8	2
Ravi	473	213	4585	4949	4761	4758	29.0	23
Sutlej	3,172	2,020	5256	5614	5436	5436	25.9	10
G. Zangbo*	55	21	5647	5930	5779	5777	23.9	3
Yamuna	176	133	4850	5309	5083	5087	29.3	16
Bhagirathi	644	830	5285	5804	5544	5543	30.9	18
Alaknanda*	606	721	5139	5626	5380	5381	29.6	23
Total	11,436	9,313	5081	5472	5275	5275	27.4	15

* The inventory does not cover all glaciers of the basin
** Weighted by area